

Automatic detection and quantitative assessment of peculiar galaxy pairs in Sloan Digital Sky Survey

Lior Shamir^{1?}, John Wallin²

1. Dept. of Comp. Sci., Lawrence Technological University
21000 W Ten Mile Rd., Southfield, MI 48075, USA

2. Dept. of Physics and Astronomy, Middle Tennessee State University 1301 E Main St,
Murfreesboro, TN 37130, USA

ABSTRACT

We applied computational tools for automatic detection of peculiar galaxy pairs. We first detected in SDSS DR7 $\sim 400,000$ galaxy images with i magnitude < 18 that had more than one point spread function, and then applied a machine learning algorithm that detected $\sim 26,000$ galaxy images that had morphology similar to the morphology of galaxy mergers. That dataset was mined using a novelty detection algorithm, producing a short list of 500 most peculiar galaxies as quantitatively determined by the algorithm. Manual examination of these galaxies showed that while most of the galaxy pairs in the list were not necessarily peculiar, numerous unusual galaxy pairs were detected. In this paper we describe the protocol and computational tools used for the detection of peculiar mergers, and provide examples of peculiar galaxy pairs that were detected.

Key words: Galaxy: general – galaxies: interactions – galaxies: peculiar – astronom-

ical databases: catalogs

[?]Email: lshamir@mtu.edu

1 INTRODUCTION

Interactions between galaxies are associated with galaxy morphology (Springel & Hernquist 2005; Bower et al. 2006), quasars (Hopkins et al. 2005), enhanced rates of star formation (Di Matteo et al. 2007; Bridge et al. 2007), quasars (Hopkins et al. 2005), and activity in galactic nuclei (Springel et al. 2008). Numerous manually crafted catalogues and classification schemes of galaxy mergers have been proposed and published (Arp 1966; Struck 1999; Schombert, Wallin & Struck 1990; Vorontsov-Velyaminov 1959, 1977; Arp & Madore 1987). Cotini et al. (2013) developed and utilized a method for automatic detection of galaxy mergers, and studied galaxy merger population to show a link between mergers and galaxies with supermassive black holes.

More recent work on interacting systems has focused on pairs of galaxies with similar redshifts and small projected distances taken from the Sloan Digital Sky Survey. In these papers, the authors have systematically examined these close pairs for evidence of an increased star formation rate (Ellison et al. 2008), elevated nuclear activity (Ellison et al. 2010), and other measurable effects that might be associated with interaction. The confounding effect in these

studies is the possibility of superpositions between galaxies in the same group. If the galaxies in a close pair have peculiar morphologies, there is a high confidence that there has been a recent interaction and the system is not just a chance superposition. However since there has been no clear objective way to define when a galaxy is “peculiar” (Naim & Lahav 1996), the objective criteria of velocity and projected distance has been the best way of analyzing a large sample of interacting pairs.

Early efforts to identify and catalog peculiar galaxies used photographic surveys. The difficulty of defining a set of objective criteria for peculiar galaxies can be illustrated by the classification schemes that have been used in these catalogs. The Catalog of Interacting Galaxies VorontsovVelyaminov (1959, 1977) contained 335 objects and placed peculiar galaxies into six primary categories: “HII-regions”, “M51 type”, “Nests”, “Pairs”, “Pseudo-Rings”, “Comets”, and “Enigmatic.” The Arp Atlas of Peculiar Galaxies (Arp 1966) was a catalog of 332 peculiar and interacting systems. There were four primary overlapping categories for these objects including Spirals, Galaxies, E and E-like Galaxies, and Double Galaxies. Within

these groups, there were 37 other subgroups including “ring galaxies”, “three-arm spirals”, “galaxies with jets”, and “double galaxies with wind effects.” Given the range of naming conventions and morphologies, the question of when a galaxy is “peculiar” has remained difficult to quantify. Catalogues of galaxy interactions have traditionally been produced by manual inspection of galaxy images by a few dedicated scientists. However as data sets have grown, the Galaxy Zoo project (and including Galaxy Zoo II and the broader Zooniverse efforts) have incorporated “citizen scientist” volunteers to classify galaxy morphologies from SDSS data (Lintott et al. 2008, 2011). Such manual analysis of galaxies using crowdsourcing was used for analyzing properties of merging galaxies (Darg et al. 2010; Casteels et al. 2013).

Aside from the questions about the completeness of these catalogs, the time needed to construct them is immense. Arp & Madore (1987) reported that it took ~ 14 years to compile and produce their catalog of ~ 6400 mergers in the southern hemisphere. In the era of robotic telescopes and digital sky surveys acquiring images of many billions of galaxies (Djorgovski et al. 2013; Borne 2013), manually crafted catalogues of mergers becomes impractical. While the morphology of most galaxy mergers is known, some galaxy mergers have peculiar morphology. Here we describe the detection of peculiar galaxy mergers by a computer algorithm mining galaxy images acquired by Sloan Digital Sky Survey.

2 METHOD

Galaxy mergers feature complex morphology that involves the shape of two or more interacting galaxies, as well as the distance and position of the galaxies in the system. Here we analyze images from Sloan Digital Sky Survey (Schneider et al. 2003).

In the first step, we downloaded $\sim 3.7 \times 10^6$ objects identified by SDSS as galaxies (object type = 3) with i magnitude < 18 . Each galaxy image was of dimensionality of 120×120 pixels, downloaded directly using DR7 Catalog Archive Server (CAS) as jpg images, and converted to 8-bit TIFF format. The magnitude threshold is used to reduce the number of images to a smaller set of the brightest objects. Downloading all these images lasted 28 days.

After the images were downloaded, a preliminary test was applied to each image to filter possible artefacts. The preliminary test rejected images in which 80% or more of the pixels were brighter than 120, or images that 80% or more of the pixels were of the same colour (green, blue or red) after applying a fuzzy logic-based colour classification transform (Shamir 2006). The test was based on the SDSS colour mapping (Lupton et al. 2004), in which large swathes of a single colour are often signs of detector saturation, and can therefore be considered artefacts. After rejecting the artefacts, $\sim 3.2 \times 10^6$ objects were left.

Then, we applied an algorithm to determine whether a certain image has two neighboring objects, or that an object had more than one point spread function in it. The detection of two separate objects was detected by first applying the Otsu binary transform (Otsu 1979) to separate the foreground from the background pixels. The Otsu binary transform is performed

by first computing the Otsu threshold (Otsu 1979). The Otsu method determines the threshold above which a pixel is considered a foreground pixel by iteratively testing each gray value, and computing the variance of the pixels dimmer than that value and the variance of the pixels brighter than the candidate threshold. The gray value that provides the minimum of the sum of the variances is the Otsu threshold (Otsu 1979). The Otsu threshold separates the foreground and background pixels regardless of linear mapping of the pixels intensity values.

The set of foreground pixels is then separated into foreground objects by counting the 4-connected objects (Shamir 2011a). The 4-connected objects are simply groups of foreground pixels such that each foreground pixel $I_{x,y}$ within the group O satisfies the condition

$\forall I_{x,y} \in O \exists (I_{x,y+1} \in O | I_{x,y-1} \in O | I_{x+1,y} \in O | I_{x-1,y} \in O)$. That is, each foreground pixel in the group has at least one neighboring foreground pixel.

If more than one object is found, the image is flagged as a candidate for a galaxy merger. If only one object is found, the object is scanned for peaks using a point spread function detection algorithm (Shamir & Nemiroff 2005a,b), and if more than one peak is found the image is considered a potential galaxy merger. The peak detection code is part of the *Wolf* open source image analysis package (Shamir et al. 2006; Shamir 2012a). It should be noted that the same technique can also be used for automatic detection of recoiling supermassive black holes.

The separation of objects with more than one peak reduced the set of $\sim 3.2 \times 10^6$ images to $\sim 4.32 \times 10^5$ potential galaxy mergers. However, many of these images are not images of interacting galaxies. Figure 1 shows a few examples of objects classified as galaxies by SDSS pipeline and were also detected as potential galaxy mergers.

As the figure shows, images with two objects or with objects with two detected PSFs are not necessarily galaxy mergers. To find galaxy mergers we used the Wndchrm image analysis software tool (Shamir et al. 2008a; Shamir 2013b), which was originally developed for analysis of microscopy images (Shamir et al. 2008b, 2010a), but was also found informative for the analysis of galaxy images (Shamir 2009), and in particular for analyzing the morphology of galaxy mergers (Shamir et al. 2013a). Wndchrm works by first extracting a very large set of numerical image content descriptors for each image, so that each image is represented by a vector of 2883 numerical values. These content descriptors provide a comprehensive set that reflects the shape, colour, textures, fractals, polynomial decomposition of the image, and statistics of the pixel value distribution. These content descriptors are extracted from the raw images, but also from transforms of the images (e.g., FFT, Wavelet, Chebyshev, gradient), as well as combinations of transforms (e.g., FFT transform of the Wavelet transform). A detailed description of Wndchrm can be found in (Shamir et al. 2008a, 2010b, 2013a). Wndchrm performs colour analysis by using the RGB channels (Shamir et al. 2010b). That type of analysis might be less accurate than analyzing the FITS images of each colour channel separately, but it allows colour analysis without the need to download multiple FITS files for each celestial object, and

therefore scales better when downloading and processing millions of galaxies.

Wndchrm was used by first manually classifying an initial set of 100 true galaxy mergers and another set of 100 images

that are clearly not mergers. Then the image classifier was used to classify the galaxy images, and was inspected for classification errors. For each misclassified image, the image was added to the training set to improve the efficacy of



Figure 1. Objects detected as possible galaxy mergers

the classification, leading to a training set of 500 samples. The training set was applied to the dataset of $\sim 4.32 \times 10^5$ galaxies, and reduced it to $\sim 2.1 \times 10^4$ images that were classified by Wndchrm as mergers. The image classification using Wndchrm takes ~ 45 seconds to classify a single galaxy image using a single core of Intel core-i7 processor, but since Wndchrm can be easily parallelized (Shamir et al. 2008a), a medium-sized cluster of 320-cores can process the galaxy images in less than one day.

To find peculiar galaxy mergers, we then applied an algorithm for automatic detection of peculiar galaxies (Shamir 2012b) that works by weighting the image content descriptors computed by Wndchrm such that the weights are determined using the variance of the values in the training set, and then measuring the weighted Euclidean distance between each image in the test set and the “typical” image in the training set. The algorithm is based on a peculiar image detection algorithm (Shamir 2013b), and was applied to galaxy images as described in detail in (Shamir 2012b). Experimental results and a detailed description about the peculiar image detection algorithm is provided in (Shamir 2012b, 2013b). From the output of the peculiar image detection algorithm we took the top 500 images and inspected them manually.

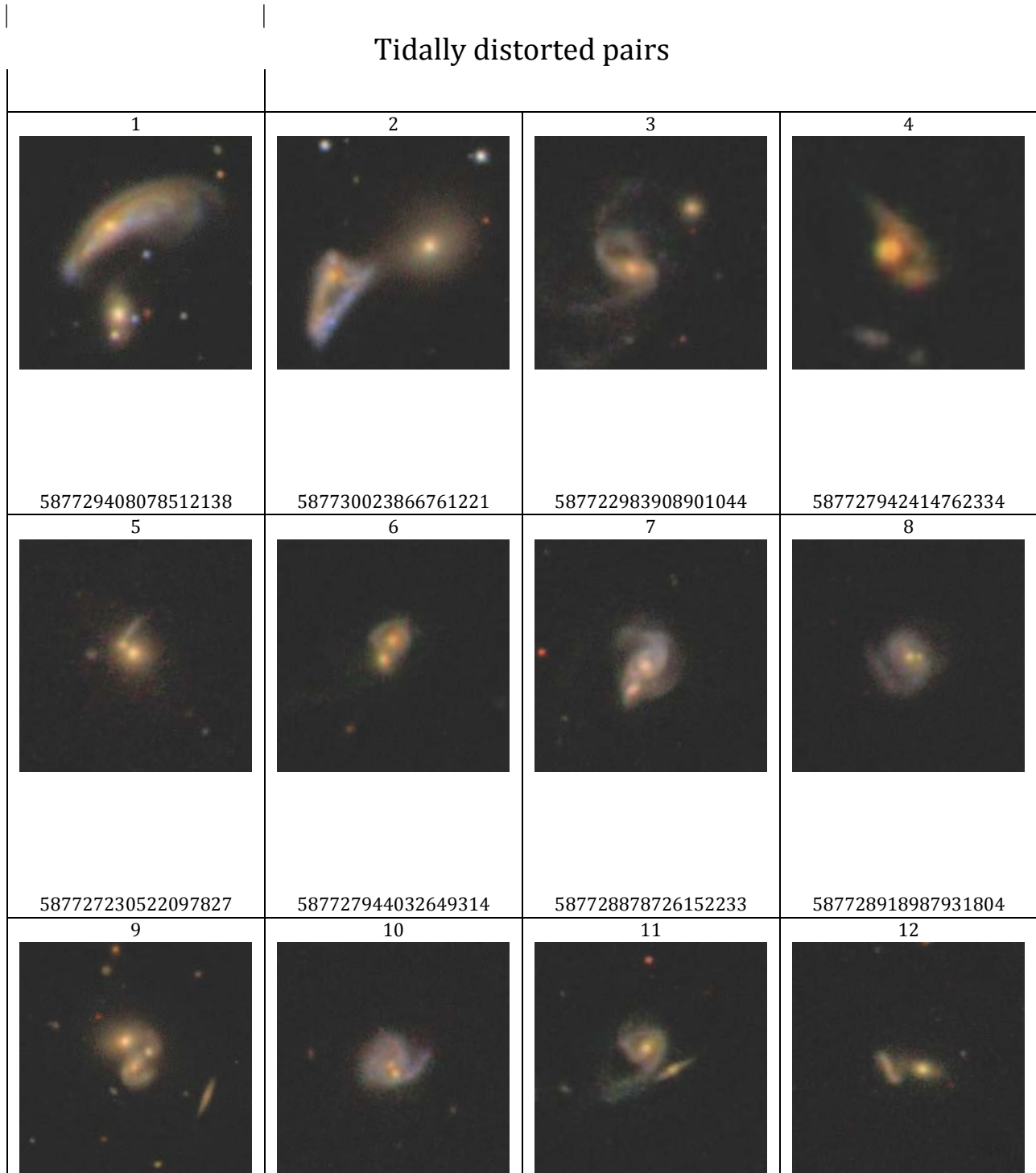
3 RESULTS

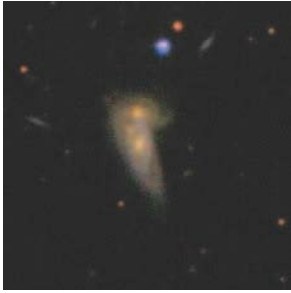

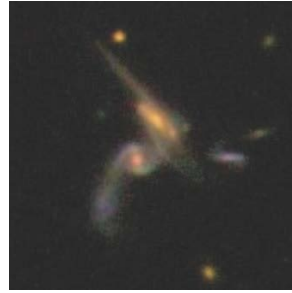

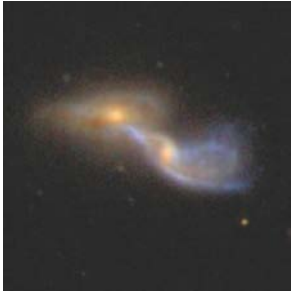
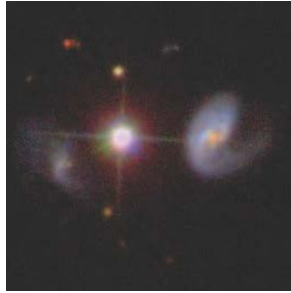

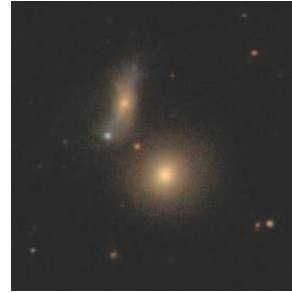
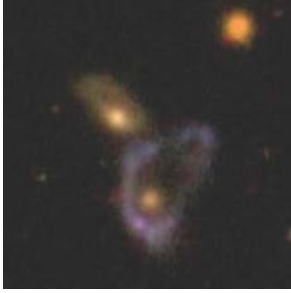

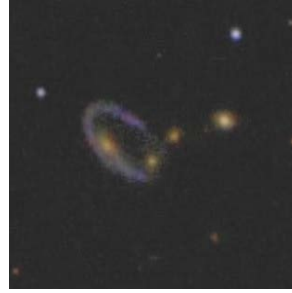

Automatic detection of peculiar galaxies is a complex task, and it is expected that such algorithms will have a certain degree of noise. Due to the noise, many of the 500 galaxy pairs detected by the algorithm were not peculiar, and some also contained artefacts that were not filtered in the previous stages. However, among the shortlist of galaxy pairs many images of peculiar galaxy pairs were found. Although the algorithm had to rely on a last step of manual inspection, it reduced a list of $\sim 3.7 \times 10^6$ images of celestial objects into a manageable list of 500 candidate objects. From that list, artefacts and non-peculiar galaxies were removed by manual examination of the galaxy pairs, and the most peculiar objects were selected manually by the authors.



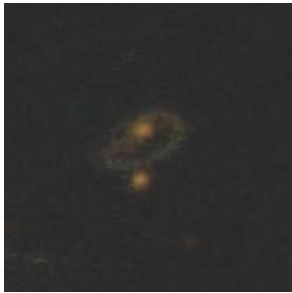

Figure 2 shows the image, DR7 object ID, and celestial coordinates of some of the objects detected by the algorithm. As mentioned above, most celestial objects in the list of 500 objects were not peculiar or did not have clear morphology, and are therefore not included in this paper. The list of 500

celestial objects is available as supplementary on-line material of this paper.


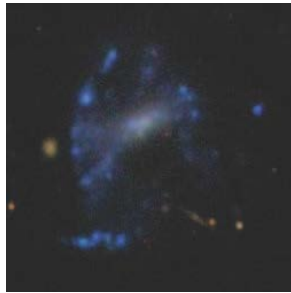
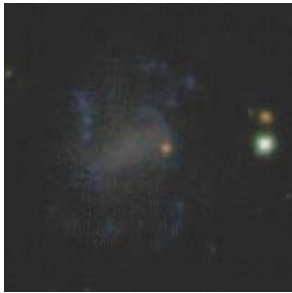




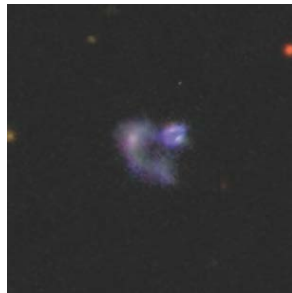
Figure 2. Examples of the galaxies identified by the method. The identification number below each galaxy image is the SDSS DR7 object identification number. The number above each image is an identifier by which the galaxy pair is identified in the paper




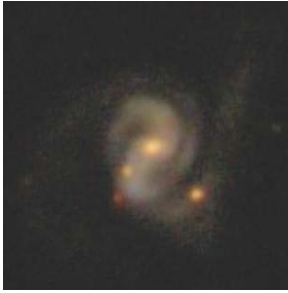








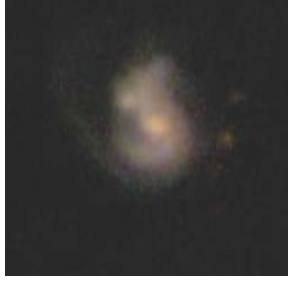

587729772070633570 13 	587739156573585582 14 	587741710474870997 15 	587742772949549151 16 
587744875857642337 17 	587746236302360825 18 	588015509281833181 19 	587736942524629287 20 
Collisional Ring Galaxies			
587730774407840452 21 	587742631737229751 22 	587730845814751853 23 	587728308567015452 24 

25	26	27	28
			
587729233595859458	587736976890134917	587731187810238739	587725550139277460

Blue Galaxies with Unusual Morphologies

29	30	31	32
			
587739305294626830	587731500262948921	587741533327458358	587739407295905821
33	34	35	36
			
587729772072861802	587732484351590536	588848900451008597	587725775608086591

Galaxies with Embedded Point Sources

<p>37</p>  <p>587729233591861508</p>	<p>38</p>  <p>587728676861182142</p>	<p>39</p>  <p>587726102561161239</p>	<p>40</p>  <p>587733434070860127</p>
<p>41</p>  <p>587742015424233553</p>	<p>42</p>  <p>587724232110440585</p>	<p>43</p>  <p>587729233051648085</p>	<p>44</p>  <p>587729653430222900</p>
<p>45</p>  <p>587733410446180362</p>	<p>46</p>  <p>587742013279502419</p>	<p>47</p>  <p>587740522398089357</p>	<p>48</p>  <p>587732134852427839</p>
<p>Edge-on Galaxies and Linear Features</p>			
<p>49</p>	<p>50</p>	<p>51</p>	<p>52</p>

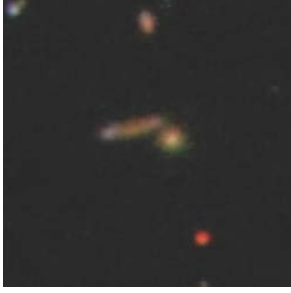





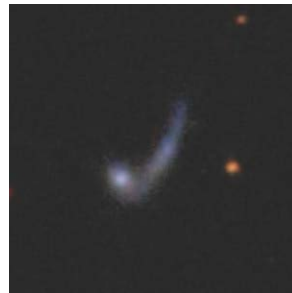


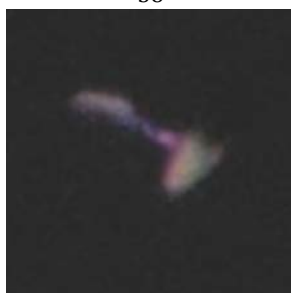

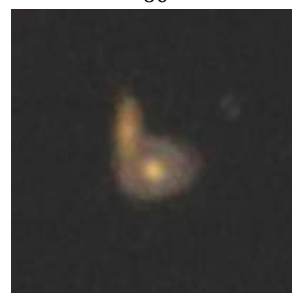
			
587729776907452608	588011219678527613	587731681724531032	587740552454340671
53	54	55	56
			
587724232104280165	587742863676473541	587732702867095573	588017704018313247
57	58	59	60
			
587741602571223188	587739380459700413	587726015607341151	587739721384264013

Table 1: Tabular data on the example galaxies.

No.	SDSS ID	RA (degrees)	Dec (degrees)	z	Descriptions and cross identifications
1	587729408078512138	249.55762	41.93106	0.028	Tidally distorted interacting pair Arp 125/UGC 10491
2	587730023866761221	222.85136042	6.80141814	0.035	Tidally distorted interacting pair [RC2] A1488+07B/CGCG 048-028N
3	587722983908901044	228.80236789	0.48465685	-	Tidally distorted interacting pair
4	587727942414762334	130.41641554	0.47482966	-	Tidally distorted interacting pair
5	587727230522097827	24.57851606	-9.53761984	0.105	Tidally distorted interacting pair
6	587727944032649314	146.96981692	2.2030615	0.100	Tidally distorted interacting pair
7	587728878726152233	146.07461364	2.82742562	0.061	Tidally distorted interacting pair

8	587728918987931804	228.93245046	57.32576843	0.069	Tidally distorted interacting pair
9	587729772070633570	204.18173946	-3.49915134	0.053	Tidally distorted interacting pair CGCG 017-034
10	587739156573585582	133.73038433	24.57972348	- 0.000	Late stage merger + second nucleus
11	587741710474870997	129.7030717	17.77376393	0.118	Tidally distorted interacting pair
12	587742772949549151	183.55630868	16.39304707	0.106	Tidally distorted interacting pair
13	587744875857642337	118.40246117	9.39599884	-	Tidally distorted interacting pair CGCG 058-063
14	587746236302360825	213.24517723	- 15.64564401	-	Tidally distorted interacting pair
15	588015509281833181	28.43139742	0.18638246	0.082	Tidally distorted interacting pair
16	587736942524629287	230.40263074	31.31348877	0.107	Tidally distorted interacting pair
17	588298664650145819	194.20114032	48.29557185	0.028	A strongly interacting pair of disk galaxies NGC 4837/I Zw 046
18	587724232641937419	20.01095866	14.36176367	0.031	Pair of tidally distorted galaxies next to a bright star CGCG 058-063
19	587731499185864817	155.94389483	53.10296621	0.031	Close pair of spirals - some evidence of tidal distortion UGC 05615/VV 312/CGCG 1020.6+5321
20	587736974735704203	231.39225706	26.55545497	0.034	Spiral + Elliptical interacting pair CGCG 165-053
21	587730774407840452	318.5274773	10.60878036	0.089	Double ring galaxy
22	587742631737229751	257.37340763	42.53970985	-	Tidally distorted interacting pair
23	587730845814751853	315.55380799	-1.19879418	0.100	Collisional ring galaxy
24	587728308567015452	172.03453114	2.3942382	-	Apparent ring galaxy?
25	587729233595859458	260.34558059	33.72469744	-	Apparent ring galaxy and intruder
26	587736976890134917	247.3840953	20.33012694	0.092	Apparent ring galaxy and pair of ellipticals
27	587731187810238739	350.15009605	1.18186531	-	Collisional ring
28	587725550139277460	188.02672417	66.40332813	0.048	Collisional ring UGC 07683/VV 788, VII Zw 466/ CGCG 315-043/[RC2] A1229+66B
29	587739305294626830	195.73997132	35.66516	0.037	Incomplete ring galaxy
30	587731500262948921	167.90750782	56.51715493	0.010	Unusual irregular galaxy
31	587741533327458358	184.20861132	30.27156024	0.013	Irregular galaxy
32	587739407295905821	126.70406448	20.36484288	0.025	Irregular galaxy IC 2373/UGC 04409/CGCG 119-100
33	587729772072861802	209.30600585	-3.36564749	-	An irregular blue galaxy next to reddish star
34	587732484351590536	155.00631865	46.59967906	0.030	An isolated irregular blue galaxy
35	588848900451008597	183.27620792	0.212918	0.096	An irregular blue galaxy
36	587725775608086591	121.73547563	48.51907092	0.078	One-armed spiral and companion
37	587729233591861508	254.77478876	41.80435125	-	Superposition between a barred spiral and a star?
38	587728676861182142	203.67710948	62.57444007	0.076	Multiarm barred spiral
39	587726102561161239	222.7289759	4.94891811	0.014	Spiral with bright star in its disk
40	587733434070860127	254.71927935	28.30197041	-	Red with star
41	587742015424233553	167.11388932	22.61855803	0.022	Blue spiral with star
42	587724232110440585	32.64724334	12.91822181	0.1	Merging pair
43	587729233051648085	248.46782084	47.99532843	0.035	Distorted galaxy with nearby star CGCG 251-028
44	587729653430222900	261.09832143	25.60862749	-	Single arm spiral and companion
45	587733410446180362	213.91507664	50.71345968	0.049	Single arm spiral and companion
46	587742013279502419	174.12239999	21.59607456	0.030	Spiral galaxy with a second nuclear source
					NGC 3758

10 Shamir & Wallin

47	587740522398089357	8.89698672	23.76797938	-	Close interacting pair with tidal distortions
48	587732134852427839	195.92079205	51.49684627	0.038	Merging pairs
49	587729776907452608	214.6336745	-2.61358823	-	Close pair
50	588011219678527613	229.9230259	54.82464843	0.115	Close pair
51	587731681724531032	122.52209047	35.16653732	0.087	Edge-on interaction of to spirals
52	587740552454340671	54.69581337	15.54806086	-	Close pair
53	587724232104280165	18.14808494	14.01249256	0.053	Close group of three galaxies
54	587742863676473541	181.80239643	16.96934309	0.072	Possible superposition? CGCG 098-060
55	587732702867095573	162.928461	7.2946855	0.023	Close pair
56	588017704018313247	212.82335434	11.3211844	0.028	Tidally distorted galaxy
57	587741602571223188	190.90262203	27.89193356	0.083	Close pair
58	587739380459700413	239.01810342	21.8666069	0.085	Close pair
59	587726015607341151	183.44198571	2.81152618	0.073	Late stage
60	587739721384264013	242.60781765	17.76026039	0.129	Possible superposition between two spiral galaxies

3.1 Characteristics of Targets

In Figure 2 we present a set of sixty images of galaxies that were detected using our method. Some of these images are clearly strongly interacting systems, while others have unusual morphologies. It would be impossible to represent all of the types of galaxies found by the algorithm, but these groupings help inform the types of features that the algorithm finds unusual enough to be flagged.

3.1.1 Tidally Distorted Pairs

Galaxies in this category are close pairs of interacting systems with obvious tidal distortion. The first set of twenty galaxies from Table 1 shows some examples of these kinds of morphologies. In images such as galaxies 1 and 2, we can see highly distorted spiral galaxies. These systems are clearly in the late stages of a merger, but rather shortly after the close approach between the galaxies in these images. The galaxies in images 5 through 9 also have strong tidal features, but seem to be examples of older interactions. In all of the examples of tidally distorted pairs, the galaxies do not follow the patterns typically associated with either spiral or elliptical galaxies, and there are two identifiable progenitors in the system with at least one showing clear signs of tidal disruption.

3.1.2 Collisional Ring Galaxies

Galaxies 21 through 28 in Table 1 are examples of collisional ring galaxies (Appleton & Struck 1996). Galaxies 21, 22, 23, 27, and 28 have very bluish colours in their rings suggesting the enhanced rates of star formation commonly seen in these systems. Galaxies 24, 25, and 26 have less well defined ring structures with less bluish colours. It is possible that these systems may have progenitors with less gas resulting in very low rates of new star formation. Other ring galaxies such as in AM1724-622 exhibit similar behavior (Wallin & Struck-Marcell 1994). In galaxy pair 28 spectroscopic redshift is available for the two blue galaxies (the ring galaxy and the galaxy in the lower left part of the field), and for both galaxies the redshift is 0.048.

3.1.3 Blue Galaxies with Unusual Morphologies

Galaxies 29 through 36 have strong blue colours and unusual morphologies. Galaxy 29 is an interacting pair that underwent an interaction similar to those that formed the collisional ring galaxies in the previous section. However, galaxies 30, 31, and 32 seems to be blue spirals with irregular structures. Galaxies 33 and 34 have no obvious features such as a nucleus or spiral arms. They are clearly elongated galaxies with blue colours.

3.1.4 Galaxies with Embedded Point Sources

Galaxies 37 through 47 have secondary point sources in their disks or envelopes. In many cases, such as galaxy pairs 42, 44, 45, 46, 47 and 48, there is a bulge-like concentration in the system. These are likely late-stage mergers. For galaxies 37, 38,

39, 40, 41, and 43, there is a clear secondary point source in the disk but its origin is less clear. In some cases this may be an embedded supernova in the galaxy or perhaps a chance superposition with a foreground star.

3.1.5 Edge-on Galaxies and Linear Features

Galaxies 49 through 60 are edge-on galaxies or galaxies with long, thin features. These elements are not technically linear, but rather thin extended features that are not typically found in galaxies. In some cases such as 49, 50, 51, and 52, these may be simple super positions of an edge-on disk galaxy with a second galaxy. There are more obvious tidal features in some of the images such as 55, 56, 57 and 58. These systems seem to have connecting bridges and tidal tails on one of the galaxies. Galaxy 59 appears to be a latestage merger.

3.2 Discussion

For most of the galaxy pairs, the categorization could be into other groups. For example, galaxy pair 60 could easily be put into the category of tidally distorted groups. Additional categories could also be created to capture some of the subgroups in these systems. It would, for example, be tempting to create separate categories of early- and late-stage mergers. However, the categories and examples we have chosen are designed to illustrate systems with common visual elements that the algorithm is likely to find unusual, and the reasons why they were flagged as morphologically peculiar.

It is also important to point out that some of these galaxies have been seen before. Galaxy 1, for example, is Arp 125. Several other of the examples appear in older catalogs of galaxies and clusters.

Given the rich variety of galaxy types, it may be possible to perform additional automated classification of the images into different subcategories if a sufficiently large sample is used for training and testing. Unsupervised learning might make it possible to better understand the features that the algorithm finds peculiar. The analysis performed in this paper was done by an image analysis method that uses very many numerical image content descriptors, and the high dimensionality of the analysis makes it highly difficult to conceptualize the criteria by which a certain combination of feature values is considered peculiar.

It can be reasonably assumed that some of the detected celestial objects may be pairs of galaxies that have no gravitational interaction, but happen to be in the same field due to super-positioning (Karachentsev 1985, 1990). Since in most cases spectroscopic z is not available for both objects, it is possible to use the photometric z to obtain rough estimation whether the two objects are part of the same system or adjacent only in projection. Having accurate velocity measurements of these objects would help remove this ambiguity, but not eliminate it completely, especially for $z < 0.1$, for which SDSS photometric redshift is less accurate. Galaxy pairs 6, 7, 16, 28, 29, 32, 57 and 59 all have the same spectroscopic z for both objects. In the case that spectroscopic z is not available, we compared the photometric redshift, and the detected galaxy pairs have similar photometric redshifts.

For instance, galaxy pair 60 has spectroscopic redshift of 0.129, and the nearby galaxy has photometric redshift of 0.134. More importantly, a larger sample of interacting galaxies with clear tidal distortions can be used to train the algorithm further to identify systems that are unambiguously interacting.

4 CONCLUSION

Autonomous digital sky surveys have been generating vast pipelines of astronomical images, leading to big astronomical databases. This form of astronomical data collection cannot rely solely on manual analysis, and requires algorithms and computer methods that can process these data and transform them into smaller and well-defined datasets that can be effectively used by humans.

Here we show how an automatic method can mine through a large dataset of $\sim 3.7 \times 10^6$ galaxy images and reduce them to a list of 500 images, containing many peculiar galaxy mergers. Detecting these peculiar mergers manually in a dataset of almost four million celestial objects is very difficult to perform manually, and can be considered nearly impractical without using automatic data analysis tools. Future digital sky surveys such as LSST will provide clear morphology of billions of celestial objects, magnifying the problem of detection of peculiar galaxies by an order of magnitude and making manual detection of such objects virtually impossible. Reduction of the data to much shorter lists as was demonstrated in this work using SDSS data will make the detection of peculiar galaxies practical, or will allow the use of citizen science (Lintott et al. 2008) to analyze such future databases.

The source code for the automatic detection of peculiar images is publicly available, and can be downloaded at <http://vfacstaff.ltu.edu/lshamir/downloads/chloe>. The source code for the *Wndchrm* method (Shamir 2013b) that computed the numerical image content descriptors can be accessed at <http://vfacstaff.ltu.edu/lshamir/downloads/ImageClassifier>.

5 ACKNOWLEDGMENTS

We would like to thank the reviewer, William Keel, for the insightful comments that helped to improve the manuscript. The computing cluster that was used to process the data was supported by NSF grants number 1157162.

REFERENCES

- Appleton, P.N. and Struck, C. 1996, *Fundamentals of Cosmic Physics*, 16, 111–220
- Arp, H., 1966, *Astrophysical Journal Supplement* 14, 1–50
- Arp, H.C., Madore, B.F., 1987, *Catalog of Southern Peculiar Galaxies and Associations*, Vol. I and II, Cambridge University Press, Cambridge, UK
- Borne, K., 2013, *Planets, Stars and Stellar Systems* (Oswalt, T. D., Bond, H. E., eds.), p. 403
- Bower, R.G., Benson, A.J., Malbon, R., Helly, J.C., Frenk, C.S., Baugh, C.M., Cole, S., Lacey, C.G., 2006, *MNRAS*, 370, 645–655
- Bridge, C.R., Appleton, P.N., Conselice, C.J., Choi, P.I., Armus, L., Fadda, D., Laine, S., Marleau, F.R., Carlberg, R.G., Helou, G., Yan, L., 2007, *ApJ*, 659, 931–940
- Casteels, K. R. V., Bamford, S. P., Skibba, R. A., Masters, K. L., Lintott, C. J., Keel, W. C., Schawinski, K., Nichol, R. C., Smith, A. M., 2013, *MNRAS*, 429, 1051–1065
- Cotini, S., Ripamonti, E., Caccianiga, A., Colpi, M., Della Ceca, R., Mapelli, M., Severgnini, P., Segreto, A. 2013, *MNRAS*, 431, 2661–2672
- Darg, D. W., Kaviraj, S., Lintott, C. J., Schawinski, K., Sarzi, M., Bamford, S., Silk, J., Andreescu, D., Murray, P., Nichol, R. C., Raddick, M. J., Slosar, A., Szalay, A. S., Thomas, D., Vandenberg, J. 2010, *MNRAS*, 401, 1552–1563
- Di Matteo, P., Combes, F., Melchior, A.L., Semelin, B., 2007, *A&A*, 468, 61–81
- Djorgovski, S. G., Mahabal, A., Drake, A., Graham, M., Donalek, C., 2013, *Planets, Stars and Stellar Systems* (Oswalt, T. D., Bond, H. E., eds.), p. 223.
- Ellison S. L., Patton D. R., Simard L., McConnachie A. W., 2008, *AJ*, 135, 1877
- Ellison S. L., Patton D. R., Simard L., McConnachie A. W., Baldry I. K., Mendel J. T., 2010, *MNRAS*, 407, 1514
- Ellison S. L., Patton D. R., Mendel J. T., Scudder J. M., 2011, *MNRAS*, 418, 2043
- Ellison S. L., Mendel J. T., Scudder J. M., Patton D. R., Palmer M. J. D., 2013, *MNRAS*, 430, 3128
- Ellison S. L., Mendel J. T., Patton D. R., Scudder J. M., 2013, *MNRAS*, 435, 3627
- Hopkins, P.H., Hernquist, L., Cox, T.J., Di Matteo, T., Martini, P., Robertson, B., Springel, V., 2005, *AJ*, 630, 705–715
- Karachentsev, I. D., 1985, *Soviet Astronomy*, 29,243
- Karachentsev, I. D., 1990, in *NASA, Marshall Space Flight Center, Paired and Interacting Galaxies*, IAU Colloq., 124, 3
- Lintott, C. J., et al., 2008, *MNRAS*, 389, 1179
- Lintott, C. J., Schawinski, K., Bamford, S., et al., 2011, *MNRAS*, 410, 166
- Lupton, R., Blanton, M. R., Fekete, G., Hogg, D. W., O’Mullane, W., Szalay, A., Wherry, N., 2004, *PASP*, 116, 816
- Naim, A., Lahav, O., 1996, *MNRAS*, 286, 969
- Otsu, N., 1979, *IEEE Trans on Syst., Man and Cyber* 9: 62–66
- Patton D. R., Ellison S. L., Simard L., McConnachie A. W., Mendel J. T., 2011, *MNRAS*, 412, 591
- Patton D. R., Torrey P., Ellison S. L., Mendel J. T., Scudder J. M., 2013, *MNRAS*, 433, L59
- Satyapal S., Ellison S. L., McAlpine W., Hickox R. C., Patton D. R., Mendel J. T., 2014, *arXiv*, arXiv:1403.7531
- Schneider, D.P., et al., 2003, *ApJ*, 126, 2579–2593
- Schombert, J. M., Wallin, J. F., Struck, C., 1990, *AJ*, 99, 497–529
- Scudder J. M., Ellison S. L., Torrey P., Patton D. R., Mendel J. T., 2012, *MNRAS*, 426, 549
- Shamir, L. Nemiroff, R., 2005a, *PASA*, 22, 111–117
- Shamir, L., Nemiroff, R. J., 2005b, *AJ*, 129(1), 539–546
- Shamir, L., Nemiroff, R. J., Torrey, D. O., Pereira, W. E., 2006, *MNRAS*, 366(2), 353–357
- Shamir, L. 2006, *Human Perception-based Color Segmentation Using Fuzzy Logic*, International Conference on Image

- Processing, Computer Vision, & Pattern Recognition, vol. 2, pp.496–505
- Shamir, L., Orlov, N., Macura, T., Eckley, D.M., Johnston, J., Goldberg, I.G., 2008a, BMC Source Code for Biology and Medicine 3, 13
- Shamir, L., Orlov, N., Eckley, D.M., Macura, T., Goldberg, I.G., 2008b, Medical and Biological Engineering and Computing, 46, 943–947.
- Shamir, L., 2009, MNRAS, 399, 1367–1372
- Shamir L, Delaney J, Orlov N, Eckley DM, Goldberg IG, 2010a, PLoS Computational Biology 6: e1000974
- Shamir L, Macura T, Orlov N, Eckley DM, Goldberg IG, 2010b, ACM Transactions on Applied Perception 7(2): 8
- Shamir, L., 2011a, ApJ, 736, 141
- Shamir, L., 2012a, WOLF: FITS file processor, Astrophysics Source Code Library, record ascl:1212.007
- Shamir, L., 2012b, Journal of Computational Science, 3, 181–189
- Shamir L, Holincheck, A., Wallin, J., 2013a Astronomy and Computing, 2, 67–73
- Shamir, L., Orlov, N., Eckley, D. M., Macura, T., Johnston, J., Goldberg, I., 2013b, WND-CHARM: Multi-purpose image classifier, Astrophysics Source Code Library, record ascl:1312.002
- Shamir, L., 2013b, Theory and Applications of Mathematics & Computer Science, 3, 13–31
- Springel, V., Hernquist, L., 2005, ApJ, 622, L9
- Springel, V., Di Matteo, T., Hernquist, L., 2008, ApJ, 620, L79
- Struck, C., 1999, Physics Reports, 321, 1–137
- Vorontsov-Velyaminov B.A., 1959. Atlas and Catalogue of interacting galaxies. Part 1. Moscow University
- Vorontsov-Velyaminov B.A., 1977, A&A 28, N1
- Wallin, J. and Struck-Marcell, C., 1994, ApJ, 433, 631–644
- Wallin, J., Holincheck, A., Borne, K., Lintott, C., Smith, A., Bamford, S., Fortson, L., 2010, ASP Conference Series, 423, 217–222